Available online at www.sciencedirect.com
SCIENCE DIRECT
Journal of Catalysis 227 (2004) 512–522
JOURNAL OF CATALYSIS
www.elsevier.com/locate/jcat

Active iron sites associated with the reaction mechanism of N_2O conversions over steam-activated FeMFI zeolites

Javier Pérez-Ramírez *

Yara Technology Centre Porsgrunn, Catalysis and Nitric Acid Technology, PO Box 2560, N-3908, Porsgrunn, Norway

Received 6 May 2004; revised 29 July 2004; accepted 6 August 2004

Available online 17 September 2004

Abstract

The relation between the intrinsic mechanism of various N_2O conversions over FeMFI catalysts and the nature of the active iron site(s) has been analyzed. To this end, direct N_2O decomposition and N_2O reduction with CO in the absence or presence of NO were investigated using a combination of transient pulse and steady-state techniques over steam-activated FeMFI zeolites with a similar iron content (0.6–0.7 wt% Fe) and different framework compositions (Si–Al, Si–Ga, Si–Ge, and Si). The forms of iron in the catalysts were characterized by UV/vis and HRTEM. The intrinsic reaction mechanism determines the optimal iron site distribution, which can be modulated by tuning the steaming temperature during activation. Oligonuclear iron oxo clusters in the zeolite channels are essential in direct N_2O decomposition due to a faster desorption of O_2 as compared to isolated ions. Such forms of active iron can be achieved at a lower steam-activation temperature over FeAlMFI and FeGaMFI (900 K) than over FeGeMFI and FeMFI (1150 K). Contrarily, zeolites with a more uniform distribution of isolated iron species lead to higher activities in N_2O reduction with CO as compared to highly clustered catalysts. In this case, O-removal as CO_2 is strongly accelerated vis-à-vis O_2 desorption in direct N_2O decomposition. The dual role of NO as a promotor in N_2O decomposition and as an inhibitor in N_2O reduction also supports the participation of different sites in both types of conversions. NO selectively inhibits N_2O reduction over isolated iron ions, further evidencing the essential role of oligonuclear iron clusters in the NO-assisted N_2O decomposition.

Keywords: N_2O decomposition; N_2O reduction; FeMFI; Framework composition; Iron species; Steam treatment; Active site; Mechanism; Kinetics

1. Introduction

The origin of the catalytic activity in reactions catalyzed by iron zeolites, and particularly the FeMFI system, has been intensively debated over the last decade. In general, the inactivity of iron ions in tetrahedral framework positions as well as of large iron oxide particles at the external surface of the zeolite crystal has been agreed upon [1–5]. The activity has been typically attributed to extraframework species confined in the zeolite pores. Two generic iron forms, isolated iron ions and oligonuclear iron clusters, have been equivocally designated as the active sites in various reactions. Different authors have considered oligonuclear iron complexes as the active sites in direct N_2O decomposition [6–8], N_2O-mediated oxidation of benzene to phenol [9–11], and selective catalytic reduction (SCR) of NO_x with hydrocarbons [12–16]. Conflictingly, other authors claim (or at least do not exclude explicitly) a preponderant role of isolated ions in these oxidation [17–20] and reduction [7,21,22] processes.

The unification of the various interpretations with respect to the active sites is extremely complicated due to the intrinsic heterogeneous constitution of iron species in the zeolite [5,7,23]. Despite considerable efforts to characterize these materials, available data are not sufficient to conclude exclusively on the structure of the active iron, particularly the nuclearity of the iron oxo clusters as well as the exact location of extraframework iron species [24]. The architecture of active clusters has been mainly hypothesized

* Fax: +47 24 15 8213.
E-mail address: javier.perez.ramirez@yara.com (J. Pérez-Ramírez).

0021-9517/$ – see front matter
doi:10.1016/j.jcat.2004.08.005

as oxygen-bridged binuclear Fe–oxo cations [10,14,15,25], although species with an average composition of Fe_4O_4 have been also reported [13]. Regardless, input from average techniques like EXAFS to determine the iron coordination should be carefully analyzed and contrasted with other characterization methods, in view of the variety of iron species in the catalyst. Application of different preparation approaches, which strongly affects the variety and relative amount of iron species, makes it more intricate. Particularly challenging in practice is suppressing clustering and precipitation of iron species, especially by application of postsynthesis methods and high iron loadings. The extraction of framework iron in isomorphously substituted Fe zeolites upon treatment in air, vacuum, or steam is claimed as a more reproducible method to disperse iron species into microporous matrices, although not allowing the insertion of a high iron content [24].

An essential aspect to be analyzed on activity determination, which has not been emphasized in the literature, concerns the application of iron zeolites in a wide range of catalytic reactions with a different mechanism. As put forward in a recent research note [7], the intrinsic mechanism of reactions involving N_2O (decomposition or reduction) determines the optimal iron site architecture. The frequent practice of designating a *universal* active site for all type of iron zeolite-catalyzed conversions is improbable by merely attending to a diversity principle. Rather, a distribution of active iron species is more plausible, which are more or less utilized depending on the mechanism and microkinetics of the particular process. In this matter, the preparation of Fe zeolites with a tailored or uniform distribution of iron species and a more detailed knowledge of the implicated reaction mechanisms would definitively lead to a better understanding of the site(s) inducing activity. The fundamental and practical relevance of the previous results in [7] deserves further investigation in order to establish a more solid generalization, since that study was confined to two zeolite samples (FeZSM-5 and Fe-silicalite), which were steam-activated at two temperatures and evaluated under steady-state conditions. Besides, no experimental evidence leading to correlations between specific mechanistic features and the preferred iron constitution was provided.

On this basis, the present work was undertaken to examine the influence of the intrinsic reaction mechanism of various N_2O conversions on the nature of the optimal iron site(s) over iron zeolites. To this end, the mechanism and kinetics of direct N_2O decomposition and N_2O reduction with CO (in the absence of presence of NO) have been elucidated by a combination of transient and steady-state techniques. This information was correlated with the iron forms in FeMFI zeolites with four different framework compositions (Si–Al, Si–Ga, Si–Ge, and Si) upon steam activation in a broad temperature range (673–1273 K). The results derived lead to an improved rational basis for catalyst design in reactions involving N_2O.

2. Experimental

2.1. Catalyst preparation

Details on the hydrothermal synthesis of the MFI zeolites with Fe–Al–Si, Fe–Ga–Si, and Fe–Si frameworks, as well as the calcinations and ion-exchange treatments previous to steam activation, have been described in previous publications [5,26]. The Fe–Ge–Si MFI zeolite was prepared following the same procedure, adding $Ge(NO_3)_3$ as the germanium source in the synthesis gel. The nominal molar metal ratios in the hydrothermal syntheses were Si/(Al or Ga) = 35, Si/Ge = 250, and Si/Fe = 150. The calcined zeolites were activated in steam (30 vol% H_2O in 30 ml STP N_2 min^{-1}) for 5 h at different temperatures, ranging from 673 to 1273 K. Throughout this paper, the catalysts are denoted making reference to the framework composition, i.e., FeAlMFI, FeGaMFI, FeGeMFI, and FeMFI, followed by the temperature of the steam treatment, e.g., FeAlMFI (873 K).

2.2. Catalyst characterization

The chemical composition of the samples was determined by ICP-OES (Perkin-Elmer Plasma 40 (Si) and Optima 3000DV (axial)). High-resolution transmission electron microscopy (HRTEM) was carried out on a Philips CM 30 T electron microscope with a LaB_6 filament as the source of electrons operated at 300 kV. The zeolites were amorphized by the electron beam in order to enhance the visibility of the small iron oxide particles. Ex situ UV/vis-DRS (diffuse reflectance spectroscopy) measurements of the steamed iron zeolites without any pretreatment were performed with a Cary 400 spectrometer (Varian) equipped with a diffuse reflectance accessory (Praying Mantis, Harrick). To reduce light absorption, samples were diluted with α-Al_2O_3 (calcined at 1473 K for 4 h) in a ratio of 1:3. The measured spectra were converted into Kubelka–Munk functions.

2.3. Steady-state studies

Catalytic activity was measured in a parallel-test unit with five fixed-bed quartz reactors (5 mm i.d.), using 50 mg of catalyst (125–200 μm) and space times of 3×10^5 and 9×10^5 g s mol^{-1} at a total pressure of $P = 1$ bar. The space time is defined as the ratio $W/F(N_2O)_o$, where W is the catalyst mass and $F(N_2O)_o$ is the molar flow of N_2O at the reactor inlet. Feed mixtures containing N_2O (1.5 mbar), CO (0–1.5 mbar), and NO (0–1.5 mbar) in He were applied. Before reaction, the catalysts were pretreated in He at 773 K for 1 h and cooled in that gas flow to the initial reaction temperature. The temperature was increased at intervals of 25 K in the range 475–900 K. This cycle was followed by a stepwise decrease of temperature in 25 K intervals. In this temperature range deactivation of the catalysts was absent and up

and down cycles lead to very similar activity curves. Generally, 1 h after a change of conditions (temperature and feed composition), the conversions of the various reactants were constant and considered as the steady state.

Steady-state kinetic studies of direct N_2O decomposition were carried out in a fixed-bed quartz reactor (7 mm i.d.) using a catalyst amount of 25–35 mg (125–200 μm), and a feed mixture of 1.5 mbar N_2O in He at atmospheric pressure. The total flow rate and reaction temperature were varied between 60 and 240 ml STP min^{-1} and 673 and 773 K, respectively. The space time was adjusted to keep the degree of N_2O conversion below 5%. This enables a proper estimation of rates of oxygen formation (molecules O_2 s^{-1} g^{-1}) according to

$$r_{O_2} = \frac{F_T C(O_2)}{W_{cat}} N_A,$$

where F_T is the total volumetric flow, $C(O_2)$ is the oxygen concentration at the reactor outlet, W_{cat} is the catalyst mass, and N_A is the Avogadro number.

The reactant and product gases were analyzed with a GC (Chrompack CP 9001) equipped with a thermal conductivity detector, using a Poraplot Q column (for CO_2 and N_2O separation) and a Molsieve 5A column (for N_2, O_2, and CO separation), and a chemiluminescence NO–NO_2 analyzer (Sigma VL). In the experiments, the mass balances of N, C, and O closed at $> 98\%$.

2.4. Transient studies

Transient experiments were performed in the Temporal Analysis of Products (TAP) reactor, a pulse technique with a time resolution in the submillisecond range. The TAP-2 reactor system has been described in detail elsewhere [27]. The catalyst (50 mg, 125–200 μm) was packed between two layers of quartz spheres of the same size fraction in the quartz reactor (6 mm i.d.). Prior to the experiments, the catalyst was pretreated in flowing He (50 ml STP min^{-1}) at 773 K and atmospheric pressure for 5 h. The pretreated sample was then exposed to vacuum (10^{-5} Pa) and pulse experiments were carried out in the temperature range of 523–823 K. Gas mixtures of N_2O:Ne = 1:1 and ^{13}CO:Xe = 1:1 were pulsed into the TAP reactor via two high-speed valves, using a pulse size of 5×10^{14} molecules (Knudsen diffusion regime). Under this diffusion regime, interaction of molecules in the gas phase is minimized, so purely heterogeneous reaction steps are investigated. In the TAP experiments, 100 pulses of the respective reactant(s) were given over the He-pretreated catalyst as a second pretreatment in order to obtain stable transient responses of the different species involved. Subsequently, 10 pulses were recorded and averaged for each AMU to improve the signal-to-noise ratio. The transient responses were typically normalized for a better comparison of pulse shapes, which is essential for deriving mechanistic insights into the reactions investigated (see Sections 3.4 and 3.5).

The gases applied in the experiments, Ne (4.5), Xe (4.0), N_2O (2.0), and ^{13}CO (99 at.% ^{13}C, Aldrich), were used without additional purification. The transient responses at the reactor outlet were monitored using a quadrupole mass spectrometer (Hiden Analytical), at atomic mass units (AMUs) related to N_2O (m/e 44), N_2 (m/e 28), O_2 (m/e 32), ^{13}CO(m/e 29), $^{13}CO_2$ (m/e 45), Ne (m/e 20), and Xe (m/e 132). The variations in feed components and reaction products were determined from the respective AMUs using standard fragmentation patterns and sensitivity factors.

3. Results and discussion

3.1. Performance of steamed iron zeolites in N_2O decomposition

Table 1 shows the chemical composition of the calcined FeMFI zeolites. The values obtained in the solids were very similar to the nominal values in the synthesis gels and did not experience significant changes upon steam treatment at different temperatures. Importantly, the samples have a very similar iron content (0.6–0.7 wt% Fe), which enables a proper comparison of performances in relation to the form(s) of iron in the catalysts.

As shown in Fig. 1, the N_2O conversion over the steam-activated iron zeolites measured at 748 K exhibits a maximum, whose position depends on the steaming temperature and the composition of the framework. Two groups of iron zeolites can be differentiated, characterized by the presence of a trivalent cation like Al or Ga or its absence. The optimal temperature is much lower for FeAlMFI and FeGaMFI (ca. 900 K) than for FeGeMFI and FeMFI (ca. 1150 K).

Steam treatment of isomorphously substituted iron zeolites is a crucial step for creating active species for N_2O activation, causing the dislodgement of framework iron to extraframework positions [3–5,19,28]. Framework Fe species are saturated with oxygen of the zeolite lattice, being unable to coordinate atomic oxygen species (from N_2O). A particular steaming temperature induces a certain distribution of iron species in the samples (Section 3.2), which determines the catalytic performance in Fig. 1. It can be tentatively reasoned that below the optimal temperature, the amount of iron in the zeolite framework represents a large fraction of the total iron in the sample (insufficient Fe extraction), while above the optimal temperature, extraframework iron has massively clustered into large iron oxide particles at

Table 1
Chemical composition of the calcined iron zeolites

Sample	Si (wt%)	Al (wt%)	Ga (wt%)	Ge (wt%)	Fe (wt%)
FeAlMFI	40.98	1.26	–	–	0.67
FeGaMFI	42.44	–	3.23	–	0.59
FeGeMFI	43.40	–	–	0.44	0.67
FeMFI	44.65	–	–	–	0.68

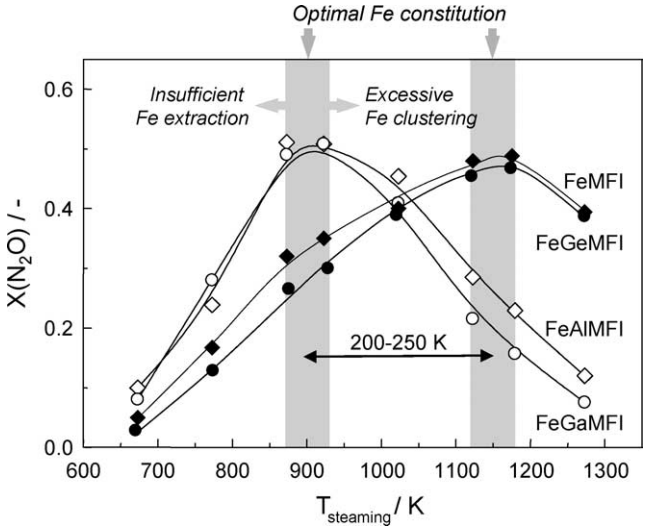

Fig. 1. N_2O conversion at 748 K vs activation temperature during steam treatment (30 vol% H_2O in N_2 flow for 5 h) over iron zeolites with different framework compositions. Conditions: 1.5 mbar N_2O in He, $W/F(N_2O)_o = 9 \times 10^5$ g s mol^{-1}, and $P = 1$ bar.

the outer surface of the zeolite crystal (excessive Fe clustering). The 200–250 K lower optimal steaming temperature in FeAlMFI and FeGaMFI for N_2O decomposition suggests that the presence of aluminum and gallium in the zeolite lattice induces an easier escape of framework iron to extraframework positions, as compared to the Ge–Si and Si lattices. In any case, the conversion over the four zeolites at optimal activation conditions is fairly similar, indicating that the catalytic activity can be modulated to the same level provided that the sample is properly activated. Consequently, a similar iron constitution in the zeolites at their optimal activation condition can be suggested.

3.2. Characterization of iron species

Characterization by ex situ UV/vis and HRTEM was applied to determine the nature and distribution of iron species and more particularly to assess the degree of iron clustering in the Fe zeolites steamed at 873 and 1173 K. These temperatures were chosen attending to the position of the optimum in Fig. 1 for both groups of samples. The visual appearance of the Fe zeolites steamed at 873 K already points to a different constitution with respect to iron. FeAlMFI and FeGaMFI are light brownish, which indicates a certain accumulation of iron oxide/hydroxide in the zeolite. FeGeMFI and FeMFI were nearly white, suggesting the more isolated nature of the iron species in these catalysts. In agreement, the HRTEM micrographs of FeAlMFI (873 K) and FeGaMFI (873 K) in Fig. 2 show the presence of iron oxide nanoparticles with a homogeneous size distribution (1–2 nm), which were not visible in FeGeMFI (873 K) and FeMFI (873 K). As reported previously [5], steam treatment of FeAlMFI and FeGaMFI at 873 K not only leads to a complete dislodgment of framework iron to extralattice positions, but also induces an extensive extraction of aluminum and gallium species by hydrolysis of SiO(H)M (M = Al, Ga, Fe) bonds. Accordingly, the presence of Al (or Ga) in the iron oxide nanoparticles cannot be totally excluded.

The UV/vis spectra of FeAlMFI (873 K) and FeGaMFI (873 K) in Fig. 3 show two intense $Fe^{3+} \leftarrow O$ charge-transfer (CT) bands at 250 and 300 nm, as well as a smaller

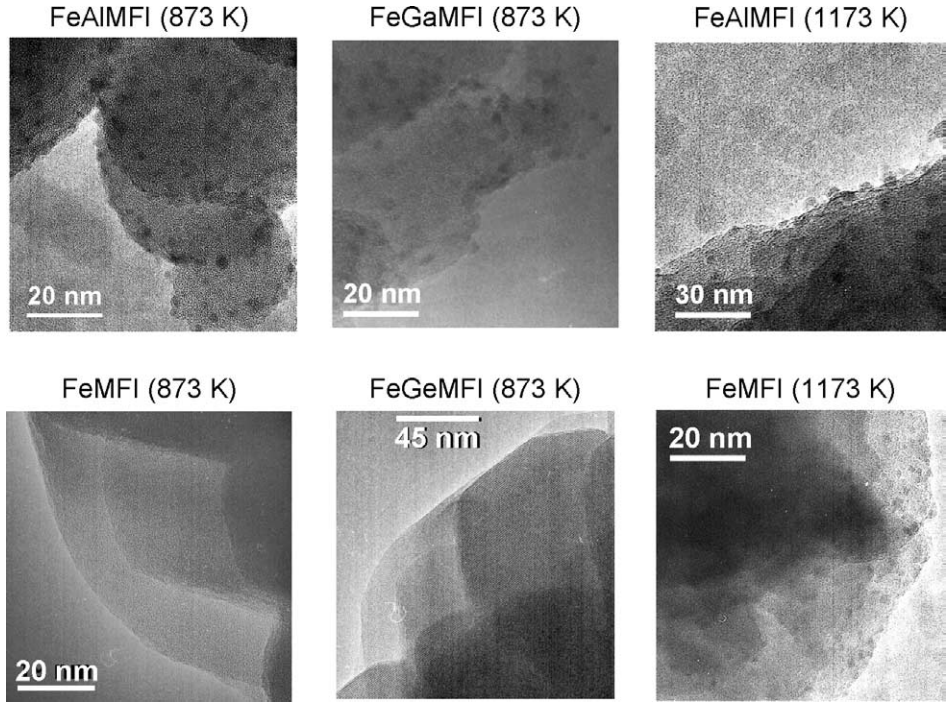

Fig. 2. HRTEM micrographs of iron zeolites steamed at 873 and 1173 K in 30 vol% H_2O in N_2 flow for 5 h.

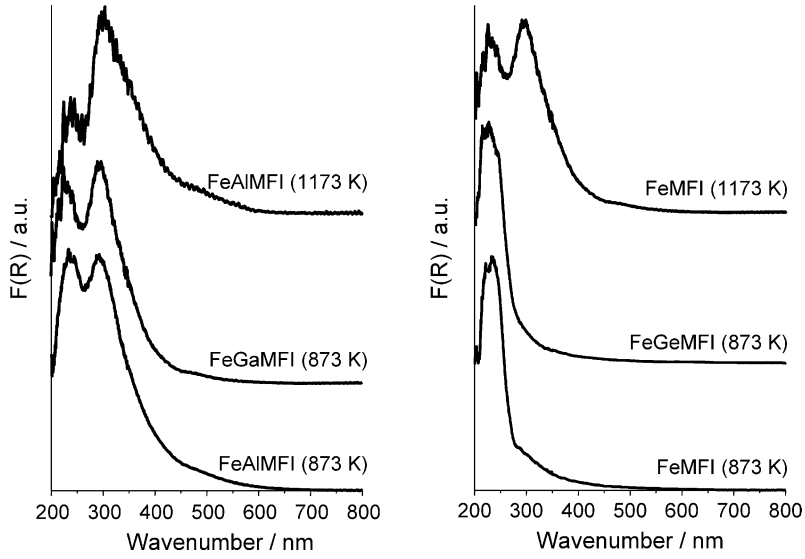

Fig. 3. UV/vis spectra of iron zeolites steamed at 873 and 1173 K in 30 vol% H_2O in N_2 flow for 5 h, without pretreatment.

contribution at 500 nm. Bands between 200 and 300 nm are typically attributed to isolated Fe^{3+} species, either tetrahedrally coordinated in the zeolite framework or with higher coordination [29–32]. Octahedral Fe^{3+} ions in small oligonuclear $Fe_x^{3+}O_y$ complexes give rise to broad bands between 300 and 450 nm and bands above 450 nm are characteristic of Fe^{3+} ions in large iron oxide aggregates [29,32], which are likely associated to the nanoparticles identified by HRTEM. Accordingly, a significant degree of iron clustering can be concluded in the Al- and Ga-containing zeolites. The UV/vis spectra of FeMFI (873 K) and FeGeMFI (873 K) display a single CT band at 236 nm, indicating that the majority of Fe^{3+} species in the samples is well isolated. The contribution at 300 nm indicates a relatively small degree of iron association in the sample in the form of oligomeric species. No contribution > 450 nm is observed, which excludes the occurrence of severe iron clustering. This is in agreement with the absence of iron oxide particles in the HRTEM micrographs of these samples in Fig. 2. Deconvolution of UV/vis bands according to the procedure described in [32] has established that the relative percentage of isolated ions, oligonuclear species, and iron oxide particles in FeAlMFI (873 K) was 30%:62%:8%, in contrast with the values obtained for FeMFI (873 K) (70%:30%:0%). This quantification did not account for the dependence of the extinction coefficient on the wavelength and the contribution of eventual Fe^{2+} present in the nonpretreated samples [32], but nevertheless provides valuable information about the distribution of the various iron species in the catalysts.

An accurate assessment of the architecture of the generically denoted Fe_xO_y oligomers cannot be provided from the above characterization. In fact, the light absorption above 300 nm in the UV/vis spectra of the clustered samples occurs in a very broad range, even overlapping with the contribution of larger Fe_2O_3 particles. This indicates the presence of a broad, heterogeneous distribution of oligonuclear clusters with different sizes and/or structures, rather than a well-defined nuclearity. Accordingly, the above-noted deconvolution of the subbands reflects a semiquantitative distribution of different cluster geometries rather than representing a certain number of different individual clustered species.

Whether the band in the high-energy range (200–300 nm) of UV/vis spectra in Fig. 3 belongs to isolated species in framework or extraframework positions cannot be a priori discerned. CT bands of tetrahedral iron incorporated in the framework of silicalite have been observed at 215 and 241 nm [29] and a band at 286 nm has been observed from isolated Fe^{3+} species in octahedral coordination in Al_2O_3 [30]. The studies in [5,26] concluded that extraction of framework iron in the Al and Ga-containing zeolites steamed at 873 K was complete and accordingly the contribution at 250–300 nm is purely attributed to extraframework isolated Fe^{3+} ions. Contrarily, a small fraction of iron remains in the zeolite framework of FeMFI (873 K), as qualitatively derived from electrochemical characterization of iron species in these zeolites [5]. A recent in situ UV/vis analysis of this sample after reduction in H_2 at 773 K has further confirmed the extensive dislodgement of framework iron species upon steaming of FeMFI at 873 K, based on distinct reduction characteristics of both types of isolated iron ions [32].

Increasing the steaming temperature of FeGeMFI and FeMFI to 1173 K leads to the complete extraction of framework iron atoms [5], obtaining light brownish samples, with a similar appearance to FeAlMFI (873 K) and FeGaMFI (873 K). This indicates iron clustering, which is substantiated by the reduced CT band associated to isolated iron ions in UV/vis, and the appearance of bands at 350 nm and at 500 nm. Associated to this, iron oxide nanoparticles are observed in the corresponding HRTEM micrographs (Fig. 2). Steam treatment of FeAlMFI and FeGaMFI at 1173 K leads to a significantly increased contribution of large iron oxide particles in UV/vis, and their average size

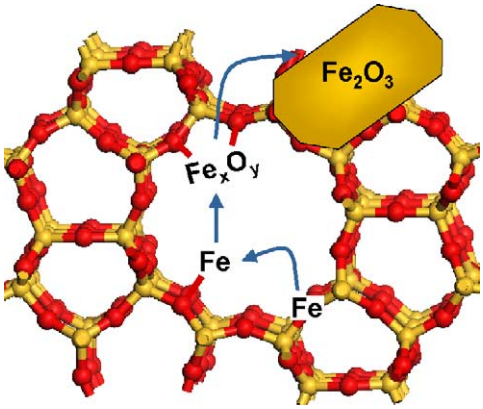

Fig. 4. Simplified scheme of the extraction of framework iron and clustering of extraframework iron species upon steam treatment of isomorphously substituted FeMFI.

is somewhat increased to 4–5 nm according to HRTEM. Deconvolution of the UV/vis subbands assigned to isolated ions, oligonuclear species, and iron oxide particles has provided relative percentages of 35%:58%:7% in FeMFI (1173 K) and of 15%:55%:20% for FeAlMFI (1173 K). The iron distributions obtained in FeMFI (1173 K) and FeAlMFI (873 K) are rather similar, further supporting the resemblance of the nature and distribution of iron species in both groups of catalysts at their optimal treatment in Fig. 1.

No definitive conclusions on the oxidation state of iron associated to these species can be drawn from the ex situ UV/vis technique applied in this study. A more extensive analysis of the redox processes associated to the iron species in the samples steamed at 873 K upon treatment in different atmospheres (air, H_2, N_2O, and CO) was carried out elsewhere by means of in situ UV/vis and EPR spectroscopies [32].

3.3. Optimal activation of iron zeolites

The mechanism of iron extraction by steaming in isomorphously substituted iron zeolites is far from being a simple and completely understood process [5,33,34]. In a simplified way, it can be considered as a clustering process as schematically shown in Fig. 4, whose extent basically depends on the steaming conditions and composition of the zeolite framework. The activation temperature should be carefully adjusted to achieve the optimal distribution of iron species, achieving the extraction of inactive framework iron but preventing extensive clustering into inactive iron oxide particles. The results in Fig. 1 unequivocally show that the conversion of the four steamed zeolites in direct N_2O decomposition is very close, provided that the samples are properly activated. Under the optimal activation conditions, both groups of zeolites investigated show a certain degree of iron association, characterized by a substantial amount of oligonuclear iron oxo clusters. However, a state with 100% of such iron without formation of iron oxide was not achieved and a heterogeneous distribution of iron species after the activation process is normally obtained. Iron clustering was largely minimized in FeGeMFI (873 K) and FeMFI (873 K), and the majority of iron is in the form of isolated ions. Clustering was not totally prevented in these samples as denoted by the contribution of oligonuclear species in the UV/vis spectra, although formation of large iron oxide particles is suppressed. Besides, a certain fraction of iron is not extracted, remaining in framework positions. These results evidence the extreme difficulty in achieving a uniform distribution of a certain iron site in Fe zeolites, although the distribution of iron species can be to some extent tailored by carefully adjusting the activation conditions.

The combination of zeolites with different lattice compositions and activation conditions with characterization and steady-state activity results enables us to conclude that the zeolites with a larger fraction of extraframework isolated iron ions are less active in direct N_2O decomposition than those with a larger fraction of oligonuclear clusters. In fact, it is well possible that the activity displayed by FeGeMFI (873 K) and FeMFI (873 K) is due to the presence of a certain fraction of oligonuclear iron species, although a contribution of isolated iron ions cannot be excluded.

The significantly lower optimal steaming temperature of the Al and Ga-containing FeMFI zeolites makes their practical application for direct N_2O decomposition more conceivable and also indicates a dramatic effect of the zeolite framework composition on the optimal activation conditions. This is a relevant point to be considered in studies claiming the superior activity of FeZSM-5 vs Fe–silicalite (and in general neutral zeolite matrices) in the N_2O-mediated oxidation of benzene to phenol [3,34–36]. These investigations have applied the same activation temperature for both framework compositions, which does not enable an equitable comparison due to their markedly different optimal steaming conditions.

3.4. Mechanism and kinetics of direct N_2O decomposition

The characterization and activity studies presented above demonstrate that the form(s) of iron in the zeolite determines the catalytic activity in direct N_2O decomposition, and subsequently triggers the question: why oligonuclear clusters are more suited to the reaction as compared with isolated iron ions.

In order to provide experimental evidence on the relationship between the intrinsic mechanism of the N_2O decomposition reaction and the optimal iron site in the Fe zeolite, transient mechanistic and steady-state kinetic studies were conducted. As generally accepted, the N_2O decomposition is initiated by the activation of N_2O on a vacant site, leading to atomic O^* species [Eq. (1)]. Two different mechanisms were postulated for regeneration of the active site [37,38]: the reaction of a second N_2O molecule with the oxidized site [Eq. (2)] and the recombination of adsorbed oxygen atoms

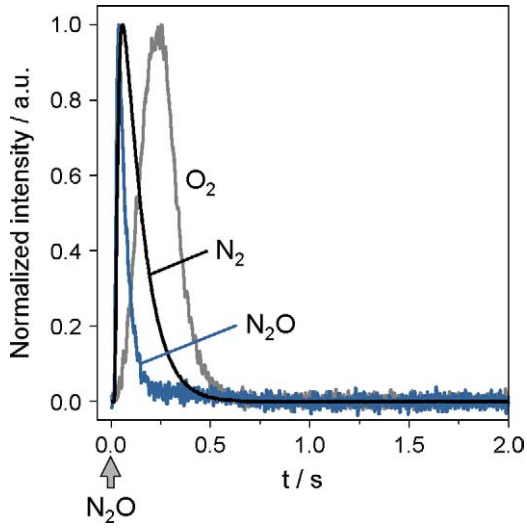

Fig. 5. Transient responses of N_2O, N_2, and O_2 during continuous pulsing of N_2O:Ne = 1:1 in the TAP reactor at 773 K over FeAlMFI (873 K).

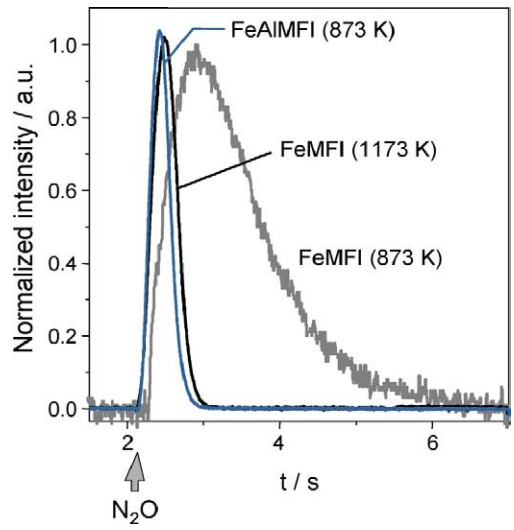

Fig. 6. Transient responses of O_2 during continuous pulsing of N_2O:Ne = 1:1 (at 2.1 s) in the TAP reactor at 823 K over steam-activated iron zeolites.

[Eq. (3)]. Since N_2O decomposition over Fe zeolites is not inhibited by O_2, Eq. (3) is considered to be irreversible [38].

$$N_2O + * \rightarrow N_2 + O^*, \quad (1)$$

$$N_2O + O^* \rightarrow N_2 + O_2 + *, \quad (2)$$

$$2O^* \rightarrow O_2 + 2^*. \quad (3)$$

The TAP reactor was used to investigate the formation of O_2 during N_2O decomposition, an essential step in the overall reaction mechanism. Under vacuum conditions in the TAP reactor, Fe zeolites decomposed N_2O without formation of gas-phase O_2 in the temperature range of 523–673 K, or gave a very broad feature, which is comparable to the noise in the mass spectrometer. Significant amounts of oxygen were observed above 773 K. Typical transient responses of N_2O, N_2, and O_2 during N_2O decomposition at 773 K over FeAlMFI (873 K) are presented in Fig. 5. The N_2 response follows directly that of N_2O, while the O_2 response is broader and considerably shifted to longer times. This important mechanistic feature indicates that during N_2O decomposition, N_2 formation is faster than O_2 formation. In this experiment, the N_2/O_2 ratio at the reactor outlet was ca. 3, indicating a certain consumption of oxygen by the zeolite.

It is widely accepted that removal of oxygen from the catalyst surface is the rate-determining step during N_2O decomposition. Accordingly, the high activity of the steamed zeolites with a certain degree of iron association in the form of oligonuclear species could be associated with the mechanism of O_2 formation. Nobukawa et al. [39] claimed the occurrence of Eq. (2) based on results from an ^{18}O-tracer technique at 693 K and atmospheric pressure over a liquid ion-exchanged FeZSM-5 catalyst. This would imply a surprising double function of N_2O as an oxidant [Eq. (1)] and as a reductant [Eq. (2)], as postulated in early N_2O decomposition studies over Fe zeolites [37]. However, in view of the uncoupling of the N_2 and O_2 responses in Fig. 5, it can be ruled out that surface oxygen species react directly with N_2O according to Eq. (2) under TAP conditions. O_2 should then be formed by the slow recombination and desorption of surface oxygen atoms, according to Eq. (3). This is in agreement with previous studies under vacuum using the Multitrack reactor in the temperature range of 573–973 K [40], and also with recent works by Pirngruber [41] over FeZSM-5 prepared by sublimation and by Bulushev et al. [42] over steamed commercial H(Fe)ZSM-5 using step-response experiments at atmospheric pressure in the temperature range of 523–673 K.

A valuable correlation can be derived between the shape of the oxygen signal during single pulsing of N_2O in the TAP reactor and the activity of the zeolites in direct N_2O decomposition. The optimally activated FeAlMFI (873 K) and FeMFI (1173 K) catalysts exhibit very similar and sharp oxygen transient responses during N_2O decomposition (Fig. 6), as compared to the broad response obtained over the less active FeMFI (873 K). This is a clear indication of an accelerated oxygen desorption process in the catalysts containing clusters, a significantly slower process in the catalysts with a larger fraction of isolated sites. The N_2O conversion in the TAP experiments was also quantified from the amount of N_2O disappeared, resulting in ca. 75% over FeAlMFI (873 K) and FeMFI (1173 K) and ca. 60% over FeMFI (873 K), evidencing a good concordance between the performance of the iron zeolites in steady-state and transient studies.

The mechanism of oxygen formation under transient conditions in vacuum can differ from that under steady-state experiments at ambient pressure. In order to bridge pulse (TAP) and flow techniques, steady-state kinetic experiments were performed in the temperature range of 623–823 K under flow conditions at 1 bar. These experiments aimed at the determination of the activation energy for oxygen formation

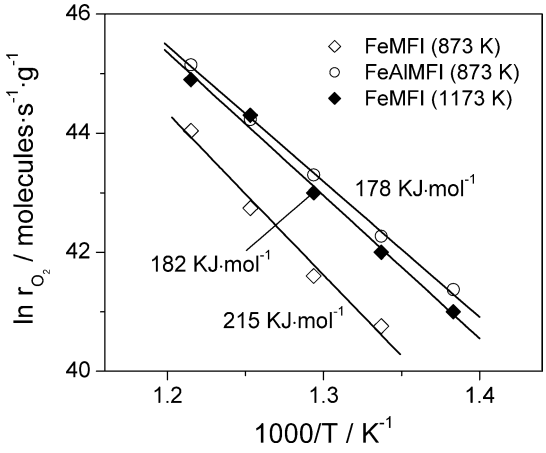

Fig. 7. Arrhenius plot of the rates of O_2 formation during N_2O decomposition over steam-activated iron zeolites. Conditions: 1.5 mbar N_2O in He and $P = 1$ bar.

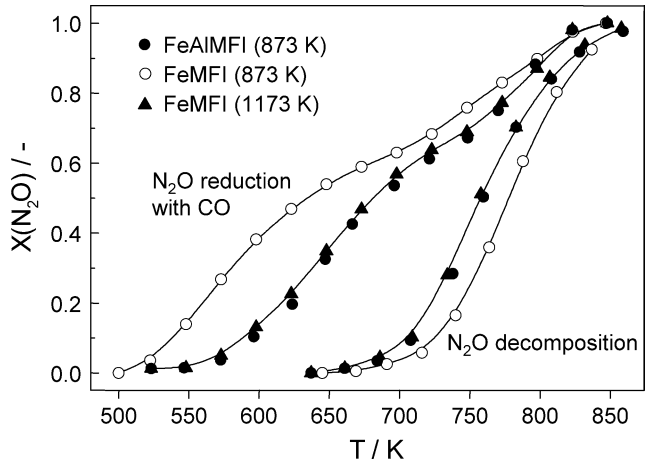

Fig. 8. N_2O conversion vs T over steam-activated iron zeolites in direct N_2O decomposition (1.5 mbar N_2O in He) and N_2O reduction with CO (1.5 mbar N_2O and 1.0 mbar CO in He). Conditions: $W/F(N_2O)_o = 9 \times 10^5$ g s mol^{-1} and $P = 1$ bar.

over differently activated catalysts. The Arrhenius plot of the rate of O_2 formation during N_2O decomposition at different temperatures is presented in Fig. 7. The results show similar reaction rates for O_2 production over FeAlMFI (873 K) and FeMFI (1173 K), as compared to the lower values over FeMFI (873 K). The apparent activation energy of O_2 formation, determined from the slope of the Arrhenius plot, is significantly higher over FeMFI (873 K) (215 kJ mol^{-1}) than over FeAlMFI (873 K) (178 kJ mol^{-1}) and FeMFI (1173 K) (182 kJ mol^{-1}). This indicates that O_2 formation during direct N_2O decomposition over FeMFI (873 K) is energetically less favorable than over the (more active) latter ones, due to a very slow recombination of atomic oxygen and thus a low rate of O_2 desorption. Thus, as regards O_2 formation during N_2O decomposition, conclusions from transient and steady-state experiments are in excellent agreement too.

The mechanistic and kinetic aspects derived from transient pulse and steady-state experiments explain the high activity of iron zeolites with a certain degree of iron association in the form of oligonuclear clusters and the relative inactivity of isolated iron ions in extraframework positions. Oligonuclear iron species appear to facilitate molecular oxygen desorption by recombination of atomic oxygen species at the lowest temperature, in view of the close proximity of iron centers as compared with isolated iron species. Isolated species may contribute at higher temperature. This would likely involve migration of atomic oxygen through the zeolite for O_2 desorption, which can be activated at a higher temperature. The mechanism of N_2O decomposition over these species may involve transport of atomic oxygen through vacancies in the zeolite matrix, which can be activated at high temperatures. In fact, not only oligonuclear iron species could act as a temporary storage for the first oxygen atom, but even the zeolite matrix can act as such, important in the case of isolated iron species. Evidence for this can be deduced from experiments with ^{18}O-labeled N_2O [43,44]. In these experiments much more ^{18}O could be accommodated in the sample than there was Fe present (∼7 times more). Iron was proposed as a "porthole" through which the ^{18}O was transferred to its direct vicinity of the zeolite matrix. Most of the oxygen will not be present as excess, but is probably exchanged; this indicates the dynamics of the oxygen in the Fe catalyst. Finally, it should be noted that not only the presence of neighboring iron ions can explain the facilitated O_2 desorption over oligonuclear clusters, but also the weaker nature of the Fe–O bond (as a result of N_2O activation) in oxo clusters as compared to isolated ions.

3.5. Reduction of N_2O by CO

Fig. 8 compares the N_2O conversion vs T of various zeolites under steady-state conditions in direct N_2O decomposition and N_2O reduction with CO. The activity of the optimally activated FeAlMFI (873 K) and FeMFI (1173 K) for direct N_2O decomposition is very similar in the whole temperature range, while the N_2O conversion over FeMFI (873 K) is shifted 40 K to higher temperatures. Addition of CO to the feed mixture lowers the operation temperature of the catalysts with respect to direct N_2O decomposition. This is generally attributed to the accelerated removal of adsorbed oxygen species from the catalyst surface in the presence of an efficient reducing agent like CO [7,45].

However, the activity order in direct N_2O decomposition and N_2O reduction with CO over the catalysts in Fig. 8 differs. In the later reaction, FeMFI (873 K) is more active than FeMFI (1123 K) and FeAlMFI (873 K), particularly in the low-temperature range (500–600 K). Above 873 K, the activity curves of the catalysts converge. Not only the N_2O conversion is enhanced over FeMFI (873 K), but also the conversion of CO to CO_2 (not shown). This indicates that conversions of N_2O and reducing agent are activated and effectively coupled, as concluded earlier [32]. In the $N_2O + CO$ mixture, a transition is visible at ca. 700 K, when the limiting reactant CO becomes exhausted (∼66% N_2O

conversion). Consequently, the N_2O conversion curve gradually shifts from N_2O reduction with CO [Eq. (4)] to direct N_2O decomposition [Eq. (5)].

$$N_2O + CO \rightarrow N_2 + CO_2, \quad (4)$$

$$N_2O \rightarrow N_2 + \tfrac{1}{2}O_2. \quad (5)$$

Pérez-Ramírez et al. [32] have recently concluded by application of in situ EPR and UV/vis spectroscopic techniques that both isolated iron ions and oligonuclear iron clusters participate in the N_2O reduction with CO over differently prepared FeMFI zeolites. The reaction mechanism is site dependent. Over isolated species, the reduction of N_2O with CO occurs via coordinated CO species on Fe^{3+} ions [Eqs. (6) and (7)], while the reaction over oligonuclear clusters proceeds via a redox Fe^{3+}/Fe^{2+} process with intermediate formation of oxygen radicals [Eq. (8)].

$$CO + * \xrightarrow{\text{Isolated site}} CO^*, \quad (6)$$

$$N_2O + CO^* \xrightarrow{\text{Isolated site}} N_2 + CO_2 + *, \quad (7)$$

$$CO + O^* \xrightarrow{\text{Oligonuclear cluster}} CO_2 + *. \quad (8)$$

An resonable correlation was found between the relative amount of isolated Fe^{3+} ions in the differently prepared Fe zeolites and their N_2O conversion indicative of a preponderant role of isolated sites in the N_2O–CO reaction [32]. Accordingly, the higher activity of FeMFI (873 K) in the reduction of N_2O with CO can be related to the relatively high concentration of isolated iron species and the minimized degree of clustering in this sample. The small remaining fraction of framework iron in FeMFI (873 K) is inactive for N_2O activation, so their controlled extraction as isolated sites could even lead to higher activity differences in Fig. 8. This is a difficult task for the reasons discussed in Sections 3.2 and 3.3.

The Temporal Analysis of Products technique was applied to investigate the mechanism of products formation during N_2O reduction with CO. To this end, N_2O:Ne and ^{13}CO:He mixtures were simultaneously pulsed over FeMFI (873 K) at 673 K (Fig. 9). Isotopically labeled ^{13}CO and nonlabeled $^{14}N_2O$ were used to uncouple the analysis of N_2O–CO_2 and CO–N_2 in mass spectrometry. The use of the most abundant isotopes for dinitrogen oxide and carbon monoxide, i.e., $^{14}N_2O$ and ^{12}CO, makes it impossible due to the identical main AMUs of $^{14}N_2O$ and $^{12}CO_2$ (44) and $^{14}N_2$ and ^{12}CO (28).

The transient responses in Fig. 9a show that the reaction products of Eq. (5), i.e., carbon dioxide and nitrogen, appear at the same time and are nicely coupled. This strongly contrasts with the delay of the O_2 response with respect to that of N_2 during single pulsing of N_2O over iron zeolites (Fig. 5). Accordingly, the rate of N_2O reduction by CO is extremely faster than that of N_2O decomposition, due to the slow recombination of adsorbed atomic oxygen species in the latter process. The difference in the tail of the $^{13}CO_2$ and N_2 responses observed in Fig. 9a has no chemical (mechanistic)

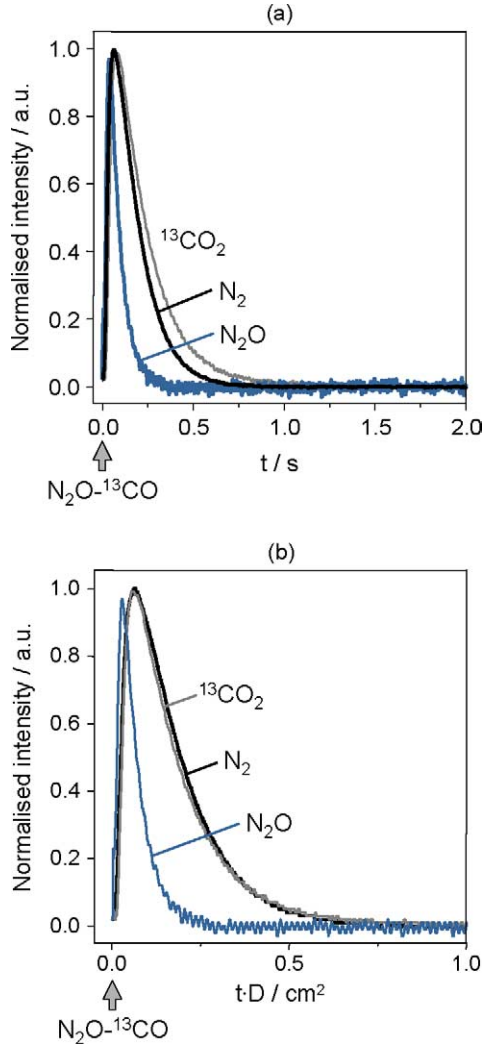

Fig. 9. Transient responses of N_2O, N_2, and $^{13}CO_2$ during simultaneous pulsing of N_2O:Ne = 1:1 and ^{13}CO:Xe = 1:1 over FeMFI (873 K) in the TAP reactor at 673 K vs (a) time or (b) time normalized by the molecular diffusion coefficient of the corresponding species.

nature, being due to the different diffusion coefficient of both species. This is demonstrated in Fig. 9b, where the profiles have been normalized by the molecular diffusion coefficient of the different species ($t\,D$), leading to identical responses. These results clearly evidence the different mechanism of O-removal in both type of N_2O conversions (decomposition and reduction), being linked with different optimal iron sites.

3.6. Influence of NO on N_2O conversions

Fig. 10 shows the effect of NO on the conversion of N_2O vs T over FeAlMFI (873 K) in different feed mixtures, containing N_2O, N_2O + NO, N_2O + CO, and N_2O + CO + NO, using equimolar amounts of the various reactants. In the absence of NO and CO, the catalyst shows significant N_2O conversions above 700 K and complete conversions at 850 K. Addition of NO enhances the N_2O decomposition activity over the catalyst, achieving similar conversions

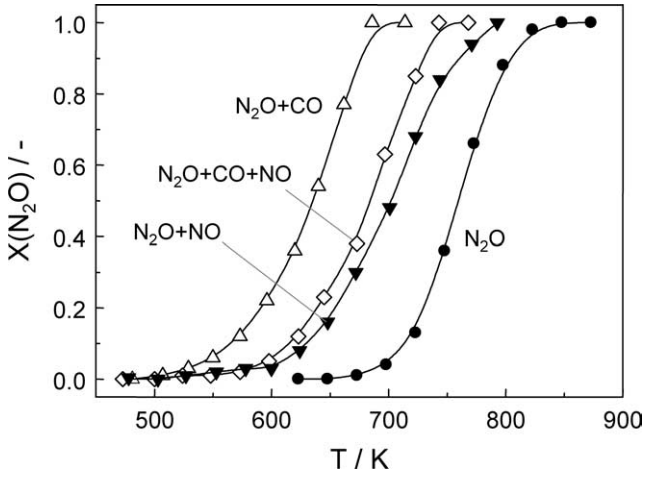

Fig. 10. N_2O conversion vs T over FeAlMFI (873 K) in (●) 1.5 mbar N_2O, (▼) 1.5 mbar N_2O + 1.5 mbar NO, (△) 1.5 mbar N_2O + 1.5 mbar CO, and (◇) 1.5 mbar N_2O + 1.5 mbar CO + 1.5 mbar NO; balance He. Conditions: $W/F(N_2O)_o = 3 \times 10^5$ g s mol^{-1} and $P = 1$ bar.

at ∼75 K lower temperature. An even significantly lower catalyst operation temperature is obtained by addition of CO to the N_2O/He feed, leading to complete N_2O conversions at 700 K, 100 K lower compared to the N_2O + NO system and 150 K with respect to the N_2O system. The presence of NO inhibits the reduction of N_2O with CO. The N_2O conversion is shifted to higher temperatures and approaches the activity of the N_2O + NO system, particularly at temperatures < 625 K. The negative effect of NO in the selective catalytic reduction of N_2O with C_3H_8 in the presence of excess oxygen has also been reported [22].

The relevance of the results in Fig. 10 focuses on the dual role of NO in N_2O conversions, acting as a promotor in direct N_2O decomposition and as an inhibitor in N_2O reduction with CO. This further supports the participation of different iron sites in both decomposition and reduction of N_2O. At low temperatures, the adsorption of NO on iron sites in the zeolite is relatively strong [46] and may block iron ions and oligonuclear iron clusters for CO and N_2O activation, respectively, so that the occurrence of Eqs. (6)–(8) is restricted. In view of the preponderance of isolated iron ions in the N_2O reduction with CO at low temperatures, it can be suggested that the inhibition occurs mainly over isolated iron sites. As a consequence of the inhibited CO activation on isolated sites, the low-temperature activity in annihilated. The N_2O conversion is shifted to higher temperatures, being dominated by the NO-assisted N_2O decomposition mechanism over oligonuclear iron species. This result nicely substantiates previous mechanistic studies [40,47], where it was concluded that NO-assisted N_2O decomposition requires a close proximity of adsorbed NO and O (from N_2O) species for a facilitated O_2 desorption via adsorbed NO_2 intermediates. The active participation of isolated iron ions in direct N_2O decomposition (with or without NO) as well as the no inhibition by NO in the reduction of N_2O with CO could be envisaged if various open coordinations would be available in these sites. However, this can be excluded based on previous infrared studies in combination with NO adsorption over the steam-activated iron zeolites [46].

4. Conclusions

Based on (i) the synthesis and characterization of iron species in steam-activated FeMFI zeolites with different framework compositions and activation conditions, (ii) testing in various N_2O conversions, and (iii) transient mechanistic and steady-state kinetic studies, relevant correlations between the intrinsic reaction mechanism and the nature of the optimal (active) iron site(s) have been derived. The results have shown that the reaction mechanism determines the preferred iron site(s), which can be modulated by tuning the steaming temperature during activation. The optimal activation is a function of the reaction in question and the framework composition of the iron zeolite. Recombination of adsorbed atomic oxygen species followed by O_2 desorption is rate-determining step in direct N_2O decomposition, being favored over oligonuclear iron oxo clusters and seriously handicapped over isolated iron ions. The mechanism of oxygen desorption from the catalyst surface strongly differs in the presence of reducing agents like CO. In this case, the rate of oxygen removal as CO_2 is much faster as compared to direct N_2O decomposition, being coupled with the rate of N_2 production. The role of isolated iron ions as active sites in the reduction of N_2O with CO is preponderant. The participation of different sites in both types of N_2O conversions reactions was also supported by experiments in the presence of NO. Apparently NO selectively inhibits N_2O reduction over isolated sites and evidence the essential role of oligonuclear iron clusters in the NO-assisted N_2O decomposition.

Acknowledgments

The author is indebted to Dr. P.J. Kooyman, Dr. A. Brückner, and Dr. E.V. Kondratenko for performing the HRTEM, UV/vis, and TAP investigations, respectively. Prof. F. Kapteijn is gratefully acknowledged for fruitful discussions.

References

[1] M. Rauscher, K. Kesore, R. Mönnig, W. Schwieger, A. Tißler, T. Turek, Appl. Catal. A 184 (1999) 249.
[2] A. Ribera, I.W.C.E. Arends, S. de Vries, J. Pérez-Ramírez, R.A. Sheldon, J. Catal. 195 (2000) 287.
[3] G.I. Panov, Cattech 4 (2000) 18, and references therein.
[4] J. Pérez-Ramírez, F. Kapteijn, G. Mul, J.A. Moulijn, Catal. Commun. 3 (2002) 19.
[5] J. Pérez-Ramírez, F. Kapteijn, J.C. Groen, A. Doménech, G. Mul, J.A. Moulijn, J. Catal. 214 (2003) 33.
[6] El-M. El-Malki, R.A. van Santen, W.M.H. Sachtler, J. Catal. 196 (2000) 212.

[7] J. Pérez-Ramírez, A. Brückner, F. Kapteijn, J. Catal. 218 (2003) 234.
[8] L. Kiwi-Minsker, D.A. Bulushev, A. Renken, J. Catal. 219 (2003) 273.
[9] G.I. Panov, V.I. Sobolev, K.A. Dubkov, V.N. Parmon, N.S. Ovanesyan, A.E. Shilov, A.A. Shteinman, React. Kinet. Catal. Lett. 61 (1997) 251.
[10] K.A. Dubkov, N.S. Ovanesyan, A.A. Shteinman, E.V. Starokon, G.I. Panov, J. Catal. 207 (2002) 341.
[11] D. Meloni, R. Monaci, V. Solinas, G. Berlier, S. Bordiga, I. Rossetti, C. Oliva, L. Forni, J. Catal. 214 (2003) 169.
[12] H.-Y. Chen, W.M.H. Sachtler, Catal. Today 42 (1998) 73.
[13] R. Joyner, M. Stockenhuber, J. Phys. Chem. B 103 (1999) 5963.
[14] H.-Y. Chen, El-M. El-Malki, X. Wang, R.A. van Santen, W.M.H. Sachtler, J. Mol. Catal. A: Chem. 162 (2000) 159.
[15] A.A. Battiston, J.H. Bitter, D.C. Koningsberge, J. Catal. 218 (2003) 163.
[16] M. Yoshida, T. Nobukawa, S. Ito, K. Tomishige, K. Kunimori, J. Catal. 223 (2004) 454.
[17] G.I. Panov, A.K. Uriarte, M.A. Rodkin, V.I. Sobolev, Catal. Today 41 (1998) 365.
[18] J. Jia, K.S. Pillai, W.M.H. Sachtler, J. Catal. 221 (2004) 119.
[19] P. Kubánek, B. Wichterlová, Z. Sobalík, J. Catal. 211 (2002) 109.
[20] S. Perathoner, F. Pino, G. Centi, G. Giordano, A. Katovic, J.B. Nagy, Top. Catal. 23 (2003) 125.
[21] F. Heinrich, C. Schmidt, E. Löffer, M. Menzel, W. Grünert, J. Catal. Commun. 212 (2002) 157.
[22] J. Pérez-Ramírez, F. Kapteijn, Appl. Catal. B 47 (2004) 177.
[23] G. Berlier, G. Spoto, G. Ricchiardi, S. Bordiga, C. Lamberti, A. Zecchina, J. Mol. Catal. A: Chem. 182–183 (2002) 359.
[24] A. Zecchina, S. Bordiga, G. Spoto, A. Damin, G. Berlier, F. Bonino, C. Prestipino, C. Lamberti, Top. Catal. 21 (2002) 67.
[25] P. Marturano, L. Drozdovà, A. Kogelbauer, R. Prins, J. Catal. 192 (2000) 236.
[26] J. Pérez-Ramírez, F. Kapteijn, G. Mul, J.A. Moulijn, A.R. Overweg, A. Doménech, I.W.C.E. Arends, J. Catal. 207 (2002) 113.
[27] J.T. Gleaves, G.S. Yablonskii, P. Phanawadee, Y. Schuurman, Appl. Catal. A 160 (1997) 55.
[28] J. Pérez-Ramírez, A. Gallardo-Llamas, J. Catal. 223 (2004) 382.
[29] S. Bordiga, R. Buzzoni, F. Geobaldo, C. Lamberti, E. Giamello, A. Zecchina, G. Leofanti, G. Petrini, G. Tozzolo, G. Vlaic, J. Catal. 158 (1996).
[30] G. Lehmann, Z. Phys. Chem. Neue Folge 72 (1970) 279.
[31] J. Patarin, M.H. Tullier, J. Durr, H. Kessler, Zeolites 12 (1992) 70.
[32] J. Pérez-Ramírez, M.S. Kumar, A. Brückner, J. Catal. 223 (2004) 13.
[33] S. Bordiga, A. Damin, G. Berlier, F. Bonino, G. Ricchiardi, A. Zecchina, C. Lamberti, Int. J. Mol. Sci. 2 (2001) 167.
[34] G. Berlier, A. Zecchina, G. Spoto, G. Ricchiardi, S. Bordiga, C. Lamberti, J. Catal. 215 (2003) 264.
[35] L.V. Pirutko, V.S. Chernyavsky, A.K. Uriarte, G.I. Panov, Appl. Catal. A 227 (2002) 143.
[36] E.J.M. Hensen, Q. Zhu, R.A. van Santen, J. Catal. 220 (2003) 260.
[37] C.M. Fu, V.N. Korchak, W.K. Hall, J. Catal. 68 (1981) 166.
[38] F. Kapteijn, J. Rodríguez-Mirasol, J.A. Moulijn, Appl. Catal. B 9 (1996) 25.
[39] T. Nobukawa, S. Tanaka, S. Ito, K. Tomishige, S. Kameoka, K. Kunimori, Catal. Lett. 83 (2002) 5.
[40] J. Pérez-Ramírez, F. Kapteijn, G. Mul, J.A. Moulijn, J. Catal. 208 (2002) 211.
[41] G.D. Pirngruber, J. Catal. 219 (2003) 456.
[42] D.A. Bulushev, L. Kiwi-Minsker, A. Renken, J. Catal. 222 (2004) 389.
[43] J. Valyon, W.S. Millman, W.K. Hall, Catal. Lett. 24 (1994) 215.
[44] J. Valyon, W.K. Hall, J. Catal. 143 (1993) 520.
[45] F. Kapteijn, G. Mul, G. Marbán, J. Rodríguez-Mirasol, J.A. Moulijn, Stud. Surf. Sci. Catal. 101 (1996) 641.
[46] G. Mul, J. Pérez-Ramírez, F. Kapteijn, J.A. Moulijn, Catal. Lett. 80 (2002) 129.
[47] G. Mul, J. Pérez-Ramírez, F. Kapteijn, J.A. Moulijn, Catal. Lett. 77 (2001) 7.